Neuroscience 365 (2017) 1–11

ADAPTATION FACILITATES SPATIAL DISCRIMINATION FOR DEVIANT LOCATIONS IN THE THALAMIC RETICULAR NUCLEUS OF THE RAT

XIN-XIU XU, YU-YING ZHAI, XIAO-KAI KOU AND XIONGJIE YU *

Zhejiang University Interdisciplinary Institute of Neuroscience and Technology (ZIINT), Qiushi Academy for Advanced Studies, Zhejiang University, Hangzhou, Zhejiang Province, China

Abstract—The capacity to identify unanticipated abnormal cues in a natural scene is vital for animal survival. Stimulus-specific adaptation (SSA) has been considered the neuronal correlate for deviance detection. There have been comprehensive assessments of SSA in the frequency domain along the ascending auditory pathway, but only little attention given to deviance detection in the spatial domain. We found that thalamic reticular nucleus (TRN) neurons exhibited stronger responses to a tone when it was presented rarely as opposed to frequently at a certain spatial location. Subsequently, we engaged signal detection theory to directly gauge neuronal spatial discriminability and found that discrimination of deviant locations was considerably higher than standard locations. The variability in neuronal spatial discriminability among the TRN population was directly related to response difference (RD) but not variance; meanwhile, further analyses attributed higher spatial sensitivity at deviant locations to larger RD. Astonishingly, a significant correlation was found between the amount of adaptation and deviant discriminability. Collectively, our results suggest that adaptation facilitates rare location discrimination by sharpening the response gap between two locations. **© 2017 IBRO. Published by Elsevier Ltd. All rights reserved.**

Key words: adaptation, novelty detection, thalamic reticular nucleus.

INTRODUCTION

The auditory environment is continuously filled with concurrent auditory stimuli, yet we can easily isolate and attend to stimuli that are novel or salient. The ability to detect these novel cues is crucial to survival in the ever-changing natural environment, but how does the brain accomplish this task? To answer this question, research has focused on either mismatch negativity (MMN), an event-related potential (ERP) signature in the central nervous system (Näätänen et al., 1978, 2007; Aghamolaei et al., 2016), or another putative mechanism for deviant and change detection (Ulanovsky et al., 2003; Yu et al., 2009b): stimulus-specific adaptation (SSA)—when a neuron adapts and even ceases responding to repeated or high-probability stimuli but maintains a comparatively strong response to less common, low-probability stimuli.

Deviance detection within the frequency domain (varying cue tone) has been studied extensively throughout the auditory pathway (Auditory cortex: Ulanovsky et al., 2003; Szymanski et al., 2009; Von Der Behrens et al., 2009; Antunes et al., 2010; Farley et al., 2010; Taaseh et al., 2011; Nieto-Diego and Malmierca, 2016; Medial Geniculate Body: Anderson et al., 2009; Yu et al., 2009b; Antunes et al., 2010; Bäuerle et al., 2011; Antunes and Malmierca, 2014; Duque et al., 2014; Inferior colliculus: Malmierca et al., 2009; Zhao et al., 2011; Ayala and Malmierca, 2012, 2015; Ayala et al., 2012; Duque et al., 2012, 2016; Pérez-González et al., 2012; Anderson and Malmierca, 2013). In contrast, much less work has been devoted to the static spatial field (varying cue location). And of those studies that did examine spatial deviants, all of them used artificial closed-field auditory cues exclusively (Reches and Gutfreund, 2008; Xu et al., 2014). Thus, to date no systematic assessment of spatial deviance detection has been carried out at the single neuron level with ecologically relevant stimuli, and as a result, it is still unknown where spatial SSA is represented in the brain.

We hypothesize that the thalamic reticular nucleus (TRN) is critical to spatial SSA. Given its strategic location between thalamus and cortex, TRN has been regarded as the ‘‘searchlight of attention” (Crick, 1984; McAlonan et al., 2008). TRN neurons exhibit strong adaptation to repetitive stimuli (Yu et al., 2009a) and show stimulus-specific responses in the frequency domain (Yu et al., 2009b). Neurons in the TRN also show binaural properties (Villa, 1990) and have been related to spatial orienting behavior (Weese et al., 1999). Taken together, the properties of these neurons are consistent with a possible role for the TRN in identifying spatially-novel stimuli. As little is currently known about spatial location

*Corresponding author. Address: Zhejiang University Interdisciplinary Institute of Neuroscience and Technology (ZIINT), Room 210, Kexue Building, Huajiachi Campus, 258 Kaixuan Rd, Jianggan District, Hangzhou 310029, China.
E-mail address: yuxiongj@zju.edu.cn (X. Yu).

Abbreviations: AC, auditory cortex; AUC, area under curve; BF, best frequency; CSI, common stimulus-specific index; ERP, event-related potential; IC, inferior colliculus; ISI, inter-stimulus interval; MMN, mismatch negativity; PSTHs, peri-stimulus time histograms; RD, response difference; ROC, receiver operating characteristic; SI, stimulus-specific index; SOP, spatial oddball protocol; SPL, sound pressure level; SSA, stimulus-specific adaptation; SSP, spatial screening protocol; TRN, thalamic reticular nucleus.

https://doi.org/10.1016/j.neuroscience.2017.09.022
0306-4522/© 2017 IBRO. Published by Elsevier Ltd. All rights reserved.

processing in the auditory sector of TRN, here we examined spatial SSA in the TRN using *in vivo* extracellular recordings from both anesthetized and awake rats.

EXPERIMENTAL PROCEDURES

Animals

All animal procedures were approved by the Animal Subjects Ethics Committees of Zhejiang University. Animals were housed in a temperature (24 ± 1 °C) and humidity (40–60%) controlled facility with a 12-h light/12-h dark cycle (lights on at 08:00). Rodent food and water were available ad libitum. Both male and female Wistar rats (260–330 g) with clean external ears were used in the current study.

Anesthesia was induced with 1.35 g/kg urethane (20% solution, i.p., Sinopharm Chemical Reagent Co., Shanghai), and the level of anesthesia was monitored by hind paw and corneal reflexes and kept stable with supplementary does of urethane (0.5 g/kg/h) as needed. In order to suppress tracheal secretion, atropine sulfate (0.05 mg/kg, s.c) was administered 15 min prior to anesthesia and a local anesthetic (xylocaine 2%) was liberally applied to the wound. Animals were prepared for surgery as previously described (Yu et al., 2009a,b; Yu et al., 2011). Briefly, subjects were mounted into a stereotaxic device and a midline incision was made on the scalp. In order to facilitate vertical access to the auditory sector of TRN, a craniotomy was made on the left hemisphere and the dura mater was removed. All recordings in the present study were from the left hemisphere. Throughout experiments with anesthesia, body temperature was maintained at 37–38 °C using a heating pad.

Following implantation of a metal head restraint, the rat was removed from the stereotaxic device and held by the head-post such that the rat was subjected to a free-field acoustic environment. For awake recordings, animals were anesthetized with pentobarbital sodium (40 mg/kg) and a fixation bar was attached to the top of skull using dental cement and six screws. A silicone elastomer was applied to the opening for protection. After recovery, rats were habituated to be head-fixed using a customized apparatus in the sound-proof chamber once every day (Schwarz et al., 2010). The animal could be monitored via a camera. The habituation period lasted 30 min for the first day, increased gradually each training session, and reached 3.5 h on the sixth day and maintained this duration on the following days. Usually, the habituation training lasted for 10 days.

Recording

Tungsten microelectrodes (Frederick Haer & Co., Bowdoinham, ME) with an impedance of 2–7 MΩ were advanced into TRN (Center: 3 mm posterior to bregma, 3.5 mm lateral to midline) via remotely operated Microdrive (MO-10, Narishige) from outside the soundproofed room according to a rat brain atlas (Paxinos and Watson, 2005). The signal was amplified and processed by TDT systems (OpenEX, TDT).

Anatomical confirmation

After the last recording, an electrolytic lesion was used to verify coordinate accuracy. The subjects were deeply anesthetized with pentobarbital sodium and transcardially perfused with 0.9% saline followed by 4% paraformaldehyde in 0.1 M phosphate buffer (pH 7.3). The brains were removed and kept overnight in 30% sucrose in 0.1 M phosphate buffer. Brains were sectioned at 50 μm and Nissl stained. Stained sections were imaged and overlaid with a physiological map with electrode penetration tracks and electrolytic lesions for guidance. Due to tissue shrinkage caused by the Nissl procedure, the Nissl images were enlarged by 10–13% prior to overlay.

Acoustic stimulation

Digital acoustic stimuli were generated with a computer-controlled Auditory Workstation (Tucker-Davis Technologies, TDT 3, Alachua, FL) and delivered through magnetic speakers (MF1, TDT). A total of 6 speakers were positioned evenly as provided in Fig. 1A (−90°, −54°, −18°, 18°, 54°, 90°) along the horizontal anterior semicircle located at the center of the rat's head with a radius of 70 cm. The sound pressure of each speaker was calibrated and set to 65 dB sound pressure level at the semicircle midpoint with a ¼″ condenser microphone (Brüel & Kjær 4954, Nærum, Denmark) as well as a PHOTON/RT analyzer (Brüel & Kjær). Upon isolation of a single TRN neuron, the stimuli below were applied:

1) Frequency screening procedure: A sequence of tones ranging in frequency from 0.5 kHz to 48 kHz was presented in random order at the right contralateral position (90°), providing 15 trials per tone. Tone duration was 100 ms with a 5-ms rise/fall time. The identified best frequency (BF) was then used for the spatial screening protocol and the spatial oddball paradigm (see below).
2) Spatial screening protocol (SSP): The BF tone was presented randomly at each of the six positions 15 times with 600 ms ISI (inter-stimulus interval) as shown in Fig. 1A.
3) Spatial oddball paradigm (SOP): We used two locations (L_1 and L_2) to come up with spatial oddball combination [L_1, L_2] ($L_1 < L_2$). The ratio of the occurrence of the standard to deviant location was 9 to 1. The tone was presented at the standard position 9 times followed by a single presentation at the deviant position. This block was repeated for a total of 20 times. Upon acquiring a single data set, the relative occurrence probability of the two locations was reversed. The ISI was 600 ms unless otherwise stated (sometimes 1s or 2s). Peri-stimulus time histograms (PSTHs; 7ms bin) were computed from over 180 and 20 trials for the standard and deviant position, respectively.

The stimuli were modified for awake subjects to shorten the recording period: we didn't include the frequency screening procedure, and we performed the

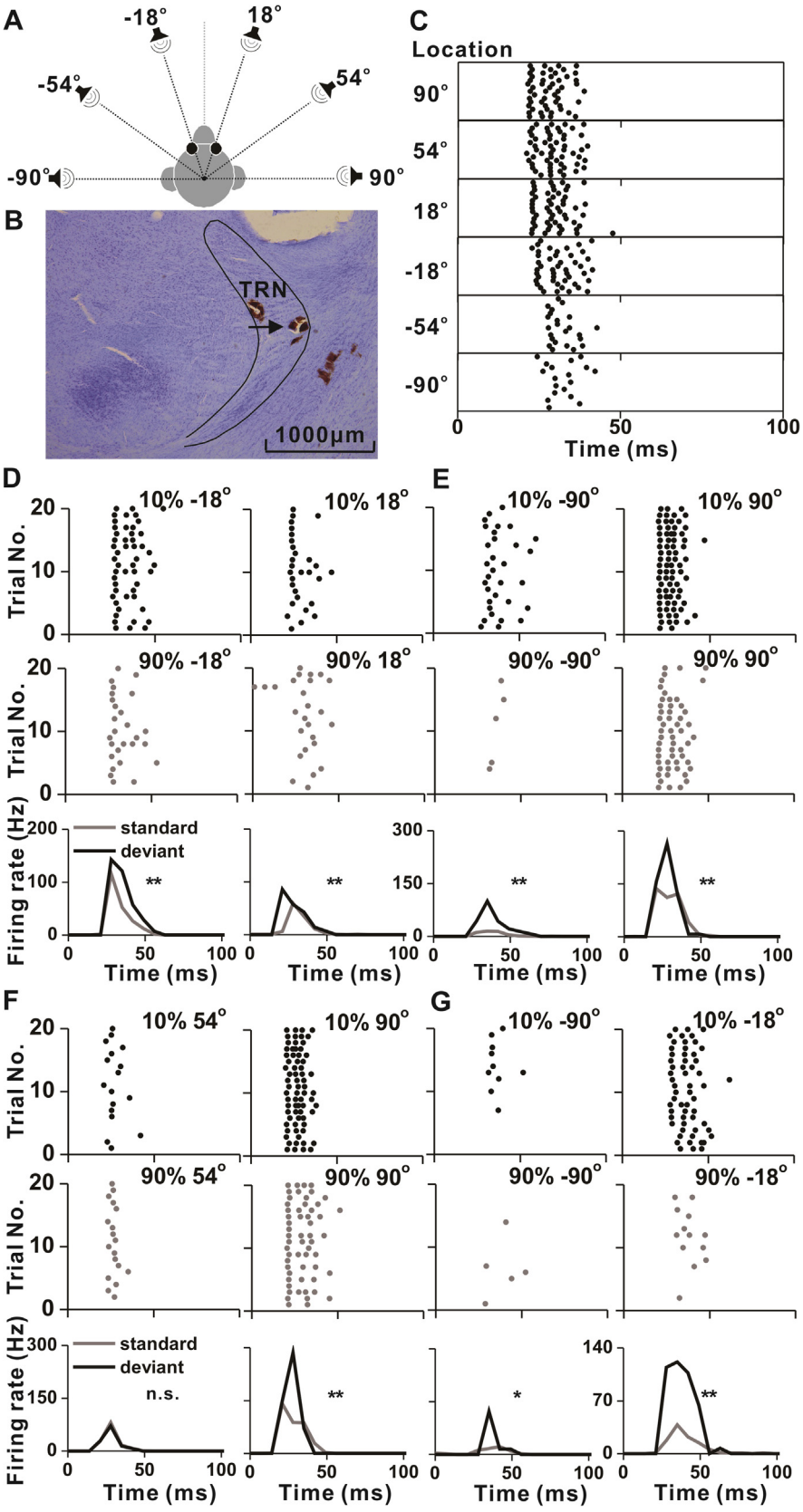

SSP and the SOP with noise bursts instead of pure tones. For the SOP, only one location combination ([−90°, 90°]) was tested, and the ratio of standard to deviant location was set to 5:1 instead of 9:1. This block was repeated a total of 30 times.

Data analysis

In order to characterize SSA in the spatial domain, we employed two published SSA indexes designed for the frequency domain (Ulanovsky et al., 2003; Malmierca et al., 2009; Yu et al., 2009b; Antunes et al., 2010): We computed an SI_i (stimulus-specific index of the location) at each location by engaging the formula: $SI_i = [d(L_i) - s(L_i)]/[d(L_i) + s(L_i)]$, with $s(L_i)$ and $d(L_i)$ being the tone responses at identical spots as standard and deviant location, respectively. We also computed CSI (Common-SSA Index), which describes the degree of SSA for the two locations and is delineated as $[d(L_1) + d(L_2) - s(L_1) - s(L_2)]/[d(L_1) + s(L_1) + d(L_2) + s(L_2)]$.

Fig. 1. Experiment setup and responses of an example TRN neuron from an anesthetized subject. (A) Six speakers were placed evenly at the frontal horizontal semicircle of the rat head (−90°, −54°, −18°, 18°, 54°, 90°). (B) Track of recording electrode, as shown by Nissl stain (the arrow indicates the recording site). Scale bar = 1000 μm. (C) Responses as a function of stimulus locations, which are shown on the left of each raster plot. Pure tones (2075 Hz) were randomly presented at six different locations, each one for 15 trials. (D–G) Raster plots and Peristimulus histograms (PSTHs) corresponding to four distinct locations combinations in the spatial oddball paradigm (D: [−18°, 18°]; E: [−90°, 90°]; F: [54°, 90°]; G: [−90°, −18°]). Raster displays showing response to tone (2075 Hz) at two locations when presented as the deviant location (black color in the top row) and the standard location (gray color in the middle row). The raster plots show the last 20 trials for standard responses, but all 20 trials for deviant responses. The occurrence probability and the sound location are indicated in the title of each plot. The PSTHs (bottom row) show the deviant (20 trials) and standard responses (180 trials). $^{*}p < 0.05$, $^{**}p < 0.01$, n.s. not significant, Wilcoxon rank test.

In addition, an ROC (receiver operating characteristic) assessment was used to determine the neuronal spatial discriminability between both locations based on neuronal responses. The AUC (area under ROC curve) offers an estimate of the neural discriminability of the two firing distributions (Von Der Behrens et al., 2009; Ayala et al., 2012; Yu et al., 2012, 2015), and ranges from 0.5 to 1, with 0.5 denoting identical firing rate distributions from locations L_1 and L_2, and 1 implying complete separation of the two firing distributions. For all spike counts, the window was always chosen from 0 to 100 ms relative to the onset of the auditory stimuli.

RESULTS

We recorded from 120 well isolated TRN neurons in 34 anesthetized rats with SOP, and 64 of those were tested with multiple location combinations. We also collected data from 8 neurons in 3 awake rats with one location combination ([−90°, 90°]) in SOP.

SSA in the spatial domain

As shown previously, TRN neurons displayed strong SSA in the frequency domain (Yu et al., 2009b). In the present study, we first examined whether or not the TRN neurons showed SSA in the spatial domain. An example neuron illustrating our procedures was shown in Fig. 1. We used an oddball paradigm with a combination of two locations. The two locations were chosen from six speakers, which were evenly distributed at the frontal horizontal semicircle centered on the head of the rat (Fig. 1A). Before that, a basic screening of the spatial responses was carried out. The example TRN neuron, with its location shown in Fig. 1B (*arrow*), responded to pure tones (2075 Hz) with fewer spikes as the sound locations moved from the contralateral site to the ipsilateral site (from the top to the bottom in Fig. 1C).

We created a spatial oddball paradigm (SOP), presenting combinations of two locations from six evenly-distributed speakers (Fig. 1A). We used 4 pairs of locations: [−18°, 18°], [−90°, 90°], [54°, 90°], and [−90°, −18°] (Fig. 1D–G, respectively). Each location in all pairs was presented as standard and deviant locations in different trials. The raster plots show responses to the tone at the same locations when the location is the deviant (top row of Fig. 1D) and when it is the standard (middle row of Fig. 1D) locations: the representative neuron showed a much stronger response at the deviant locations than that at the standard locations, and the PSTHs (bottom row of Fig. 1D) reveal a significant difference between deviant and standard responses at both locations (−18°: $p < 0.001$; 18°: $p < 0.001$. Wilcoxon rank test). Similar results were found in the other three location combinations for the same TRN neuron (Fig. 1E-*G*).

Interestingly, the deviant response at −90° location of [−90°, 90°] in Fig. 1E was considerably stronger ($p < 0.001$, Wilcoxon rank test) than when the same location (and tone) was the deviant in another location combination [−90°, −18°] (Fig. 1G). This finding suggests that responses to spatial deviance may be dependent on the spatial context.

And we also examined eight TRN neurons from three awake subjects and found similar response patterns. Data from two of the eight neurons are presented in Fig. 2. Those two neurons also exhibited stronger responses at the deviant locations as observed in the anesthetized subjects (Fig. 1).

The population-level analysis of data from anesthetized subjects is summarized in Fig. 3 and included 102 neurons in [54°, 90°], 57 neurons in [18°, 90°], and 39 neurons in [−90°, 90°]. Scatter plots of the location-specific index SI_1 versus SI_2, reveal that most values fell within the upper right quadrant (Fig. 3A), similar to previous reports from the frequency domain (Malmierca et al., 2009; Yu et al., 2009b; Antunes et al., 2010; Farley et al., 2010). This relationship, however, broke down for the location combinations [18°, 90°] and [54°, 90°] with about 42% of neurons falling within the upper left quadrant (24/57, Fig. 3B; 43/102, Fig. 3C). Those neurons had negative SI_1 and positive SI_2, parallel to the findings in the frequency domain when the frequency gap was relatively small (Ulanovsky et al., 2003; Malmierca et al., 2009; Antunes et al., 2010). Statistical comparison of SI_2 and SI_1 found no difference between SI_2 and SI_1 in [−90°, 90°] but there was a significant difference in [18°, 90°] and [54°, 90°] (SI_2 vs SI_1: $p = 0.43$, Fig. 3A; $p = 0.002$, Fig. 3B; $p < 0.001$, Fig. 3C.; signed rank test), suggesting that firing rate-related non-specific adaptation played a role in the spatial oddball responses as in previous reports of responses to the intensity oddball (Fig. 2C in Duque et al., 2016).

It is also important to highlight that the SI_2 in Fig. 3A–C described the specific index for identical location (contralateral site, 90°), yet SI_2 in [−90°, 90°] was larger than that in [18°, 90°] (ANOVA, post hoc Tukey's test: $p < 0.05$) and [54°, 90°] ($p < 0.01$), signifying that the location-specific adaptation was also spatial-context dependent. To further explore spatial context dependent firing in TRN, we compared deviant firing at the same location (contralateral site, 90°) under two or three different spatial backgrounds for each neuron (Fig. 3D). Only neurons recorded with at least two location combinations were included for this analysis ($n = 64$, Fig. 3D). 20 of 64 TRN neurons showed significantly different responses to the same deviant tones at the same locations when the spatial context (i.e. the standard location) was different ($p < 0.05$, ANOVA).

A direct comparison of the neuronal adaptation strength via the Common-SSA index (CSI) across the three conditions revealed that the CSI in [−90°, 90°] is considerably larger than that in the other two combinations (ANOVA, post hoc Tukey's test: $p < 0.0001$, Fig. 3E). For the three pairs, CSIs were all significantly higher than zero (*t*-test: $p < 0.01$), implying that on average the deviant stimulus elicited an enhanced response compared to the standard stimuli: spatial SSA was found in the TRN population under all three conditions. To eliminate the possibility that the disparity in CSI could result from diverse neuronal populations and to assess the relationship in CSI among

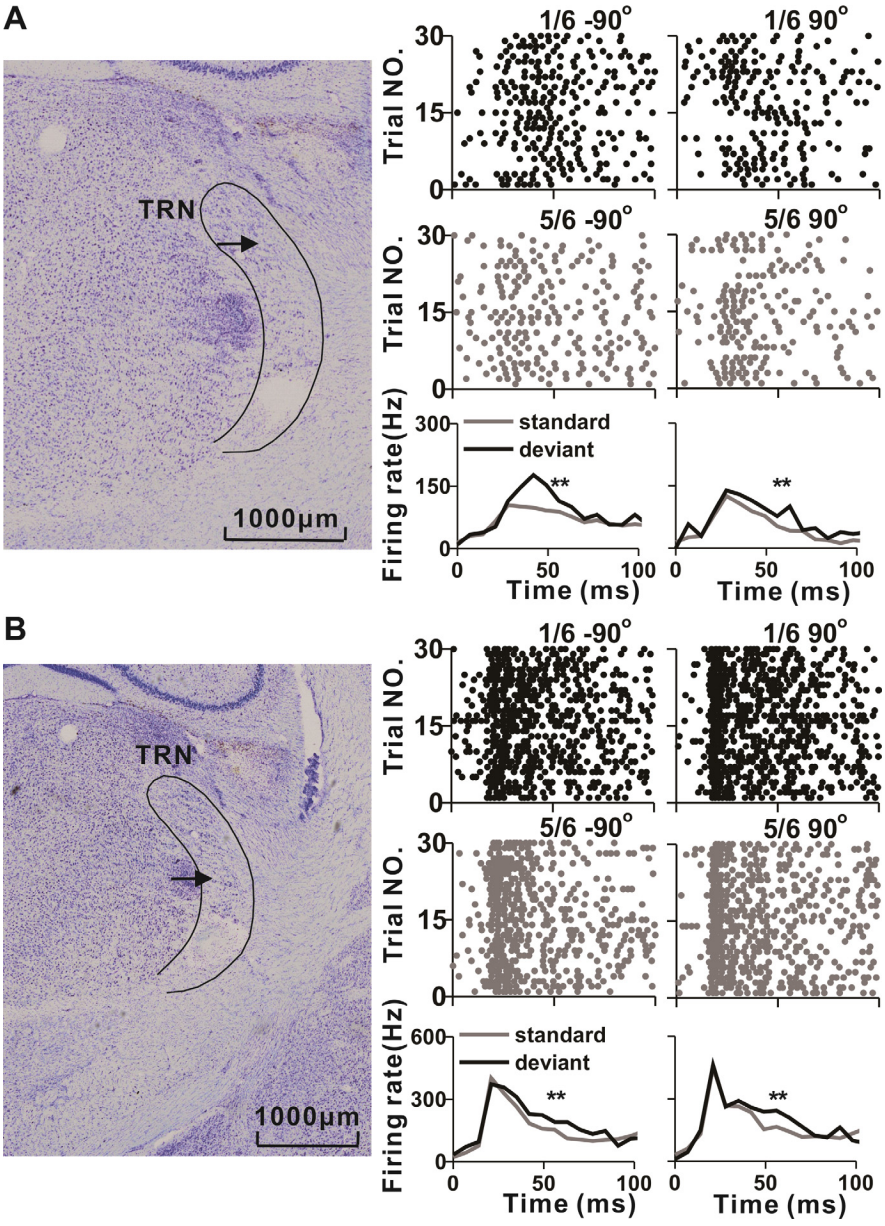

Fig. 2. Responses of two example TRN neurons from an awake subject. (A, B) Two example TRN neurons recorded from the same awake subject. Left panel: Track of recording electrode, as shown by Nissl stain (the arrow indicates the recording site), Scale bar = 1000 μm. Right panel: Raster displays showing the neuronal response to noise burst at two locations when presented as the deviant location (black color in the top row) or the standard location (gray color in the middle row). The occurrence probability and the sound location are indicated in the title of each plot. The raster plots show the last 30 trials for standard responses, and all 30 trials for deviant responses. The PSTHs (bottom row) show the deviant (30 trials) and standard responses (150 trials). $^{*}p < 0.05$ and $^{**}p < 0.01$, Wilcoxon rank test.

the different location combinations, we plotted CSI of a single location combination against another location combination and directly compared them (Fig. 3F, G). The CSI in [−90°, 90°] was greater than that in [18°, 90°] (Fig. 3F, $p = 0.003$, $n = 21$, signed rank test) and [54°, 90°] (Fig. 3G, $p < 0.001$, $n = 32$, signed rank test). No difference was found between [54°, 90°] and [18°, 90°] ($p = 0.96$, $n = 47$, signed rank test). Furthermore, the CSIs of different location combinations were positively correlated (Pearson correlation. Fig. 3F, [−90°, 90°] vs. [18°, 90°], $r = 0.67$, $p < 0.001$; Fig. 3G, [−90°, 90°] vs. [54°, 90°], $r = 0.65$, $p < 0.001$; [18°, 90°] vs. [54°, 90°], $r = 0.62$, $p < 0.001$), indicating that CSI reflects a neuronal property of spatial SSA.

The effect of ISI on spatial SSA

After identifying spatial SSA, we examined the temporal window of spatial SSA by varying ISI. When ISI was longer, the difference between the standard and deviant responses decreased in both locations as shown in Fig. 4A–C, and the CSI was weaker (CSIs were 0.42 at 600 ms ISI in Fig. 4A, 0.27 at 1000 ms ISI in Fig. 4B, and 0.15 at 2000 ms ISI in Fig. 4C). For the SI_2 versus SI_1 scatter plot, the distribution of shorter ISI's deviated more from the diagonal, showing stronger spatial SSA (Fig. 4D) as seen in the frequency domain (Ulanovsky et al., 2003; Malmierca et al., 2009; Antunes et al., 2010). The CSIs of different ISIs were also directly compared and showed that the CSI for the shortest ISI was significantly different than both longer ISIs, and that the CSI for the two longer ISIs did not differ from one another (Fig. 4E; 600 ms ISI vs. 1000 ms ISI: $p < 0.001$; 600 ms ISI vs. 2000 ms ISI: $p < 0.001$; 1000 ms ISI vs. 2000 ms ISI: $p = 0.47$, signed rank test).

Adaptation increased spatial discriminability for deviant locations

After examining the basic characteristics of spatially-deviant responses, we next explored whether and how adaptation shaped the neuronal spatial discriminability, especially for relatively close locations such as [54°, 90°]. In the frequency domain, deviant stimuli usually entail much better frequency discrimination (Von Der Behrens et al., 2009; Ayala et al., 2012). We therefore sought to compare neuronal spatial discrimination between adapted states (standard stimuli) and non-adapted states (deviant stimuli). Neuronal discriminability was quantified by AUC of the ROC curve, which is a measure of how well two distributions can be told apart by an ideal reporter and therefore an

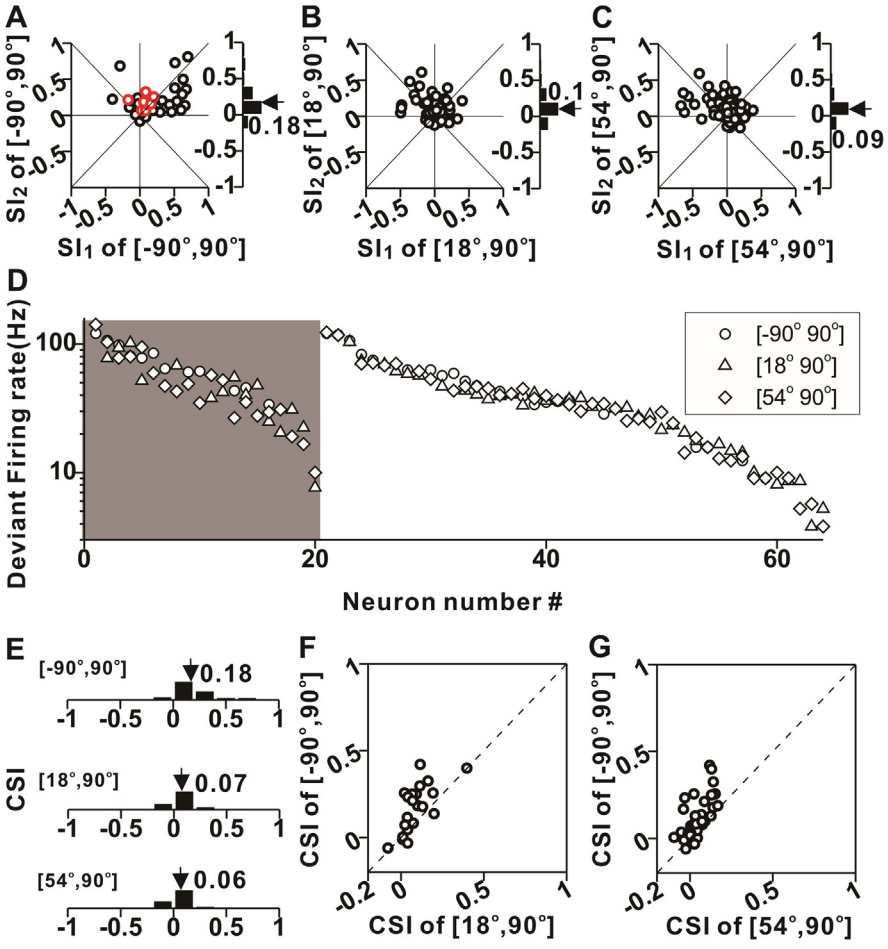

Fig. 3. Dependence of spatially deviant response on the location combination. (A–C) Scatter plots of spatial stimulus-specific index at location 2 (SI_2) versus spatial stimulus-specific index at location 1 (SI_1). Location 2 is always 90° while location 1 is −90° (A), 18° (B), and 54° (C). The red color in Figure A indicates the neurons recorded from awake rats. The marginal histograms on the right show SI_2 distribution, the arrows and the numbers illustrate the means. (D) Deviant responses at 90° of three location combinations ([−90°, 90°]: circle; [18°, 90°]: triangle; [54°, 90°]: diamond) are presented for neurons with at least two location combinations and separated into two groups: grey background (n = 20) and white background (n = 44). Each neuron in the grey background showed a significant difference in the deviant response at 90° of different tested location combinations (p < 0.05, ANOVA) while neurons in the white background did not. Both groups were sorted according to the firing rate in descending order. (E) Comparison of CSI for different location combinations. (F, G) Correlation and comparison of CSIs for different location combinations (F: [−90°, 90°] vs. [18°, 90°], n = 21; G: [−90°, 90°] vs. [54°, 90°], n = 32). The dashed line in each plot is the unity slope.

indicator of spatial discriminability in this case. The firing distribution of standard locations in an example neuron (Fig. 5A, top panel) overlapped a little, but separated completely for the same locations when they were presented as deviant locations (Fig. 5A, bottom panel). These distribution comparisons resulted in two different ROC curves (Fig. 5B): the AUC was 1 for deviant locations and 0.88 for standard locations. At the population level, the mean deviant AUC was 0.75, 11% bigger than the standard AUC for the [54°, 90°] combination (Fig. 5C, p < 0.001, n = 102, signed rank test). Similar results were obtained from the other two location combinations (deviant AUC vs. standard AUC, p < 0.01 for both [18°, 90°] and [−90°, 90°], signed rank test). The enhancement of spatial discriminability for deviant locations can also be detected from the comparison of AUC of the deviant locations in SOP with that of the same two locations in the spatial screening procedure (SSP): the AUC of the deviant locations in SOP was significantly greater than in SSP (Fig. 5D, p < 0.001, n = 102, signed rank test) although the neuronal firing rate was much greater in SSP (p < 0.001, signed rank test).

AUC depends on two properties that regulate how much the two distributions overlap: the response difference (RD) in their means and their width (variance) (Fig. 5A). The RD represents how distant the two distributions are from one another, while the variance represents the distributions' spread. In principle, high sensitivity could either be attributable to a large RD or a low variance, so each of these factors was considered separately. Fig. 6A, B plots AUC for deviant locations as a function of RD and variance, respectively. A significant correlation existed for RD (Fig. 6A; p < 0.001, type II regression) but not for variance (Fig. 6B; p = 0.59, type II regression). Similar results were found for standard locations (RD: Fig. 6C; p < 0.001, type II regression; variance: Fig. 6D; p = 0.51, type II regression), and for responses in SSP (RD: Fig. 6E; p < 0.001, type II regression; variance: Fig. 6F; p = 0.66, type II regression).

We next determined which factors gave rise to the higher sensitivity for deviant locations. Fig. 7A, B compares RD and variance from the same two locations as the deviant locations or as the standard locations, respectively. The geometric mean of RD in the deviant locations was 54.3% bigger than that in the standard locations (Fig. 7A; p < 0.001, signed rank test), and the geometric mean of the variance in the deviant locations was 9.6% smaller (Fig. 7B; p = 0.01, signed rank test), suggesting that the increase of RD and the decrease of variance may together lead to higher sensitivity to deviant locations compared with standard locations. However, when compared with SSP, a significant difference existed only for RD (Fig. 7C; signed rank test, p < 0.001) but not for variance (Fig. 7D; signed rank test, p = 0.91), suggesting that the increase of RD contributed more to the higher sensitivity of deviant stimuli, at least as compared with SSP. Similar results were also found in the other two location combinations (deviant RD vs. standard RD, p < 0.05 for both [18°, 90°] and [−90°,90°], signed rank test).

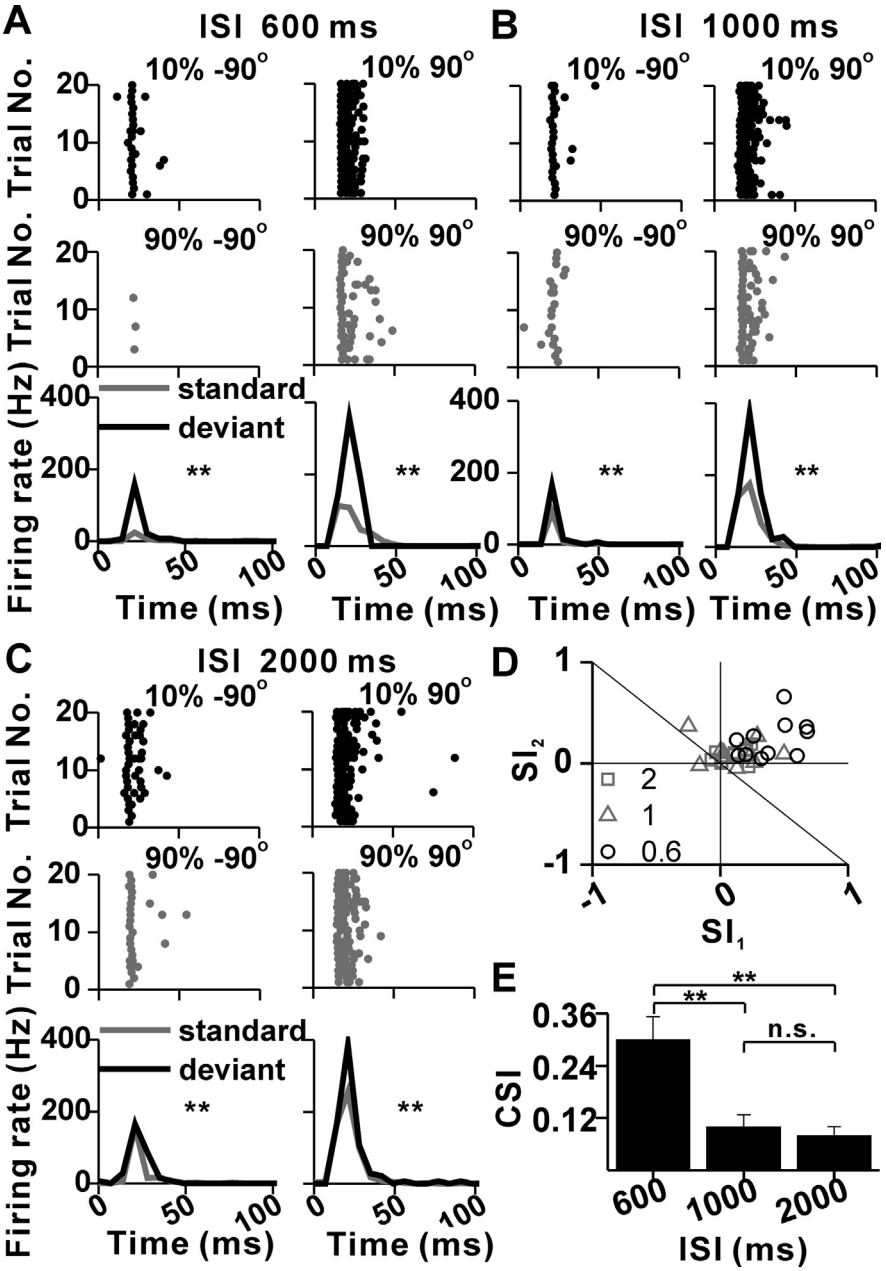

Fig. 4. Dependence of spatial SSA on ISI. (A–D) An example TRN neuron responding to the same spatial oddball protocol under three different ISIs: 600 ms (A), 1000 ms (B), and 2000 ms (C). In each figure, raster displays showing response to the tone (6912 Hz) at two locations (as indicated in each panel) when presented as the deviant location (black color in the top row) or the standard location (gray color in the middle row). The PSTHs (bottom row) show the deviant and standard responses. $^{*}p < 0.05$ and $^{**}p < 0.01$, Wilcoxon rank test. (D) Scatter plots of SI_2 versus SI_1 under three ISIs: 600 ms (black circle), 1000 ms (gray triangle), and 2000 ms (gray square). (E) CSI comparison for different ISIs (Signed rank test, $^{**}P < 0.01$; $^{*}P < 0.05$; n.s. not significant).

Association between the strength of spatial SSA and spatial discriminability

Since spatial SSA could increase the neuronal discriminability for deviant locations, the relationship between CSI and AUC is of interest. Indeed, there was a strong correlation between the degree of adaptation (CSI) and the spatial discrimination (AUC). Neurons with higher CSI tended to have superior discriminability for the deviant sites (Fig. 8A: $p < 0.001$, $r = 0.38$, Type II regression). The greater the spatial SSA, the more precisely the neuron differentiated between the two locations based on the deviant responses. Interestingly, significant correlations for the relationship between AUC and CSI were also detected in standard locations (Fig. 8B: $p < 0.001$, $r = 0.34$, Type II regression), and there was no correlation between AUC from SSP and the corresponding CSI in SOP ($p = 0.58$, Type II regression). Together, these data imply that spatial SSA shaped the spatial discriminability for standard locations in addition to deviant locations.

DISCUSSION

This study examined spatial SSA of TRN neurons and their spatial discriminability. We found that TRN neurons showed SSA in the spatial domain, and that it was dependent on spatial context. Further, spatial adaptation increased neuronal spatial discriminability for deviant locations by sharpening the response difference (RD) of the two locations.

SSA in the spatial domain versus the frequency domain

SSA has been found and studied primarily in the frequency domain, along the entire auditory pathway (see Malmierca et al., 2014; Khouri and Nelken, 2015, for review). The spatial SSA we describe here shares many traits with frequency SSA. It is worth noting, however, that this is the first exploration of spatial SSA in a free-field acoustic environment at the single neuronal level and much work remains to be done in different brain areas. Nonetheless, the observed similarities between frequency and spatial SSA are noteworthy. First, frequency CSI increases as the two tones become more different (Δf), just as we observed that spatial CSI increased as the two locations became more distant (Δl, Fig. 3E). Second, both the frequency CSI and the spatial CSI decreased as ISI increased, and both showed significant SSA even with ISI at the seconds level (Fig. 4); Third, for both cases, the scatter plot of SI_2 vs. SI_1 distributed symmetrically along the unitary line when the $\Delta f/\Delta l$ was large,

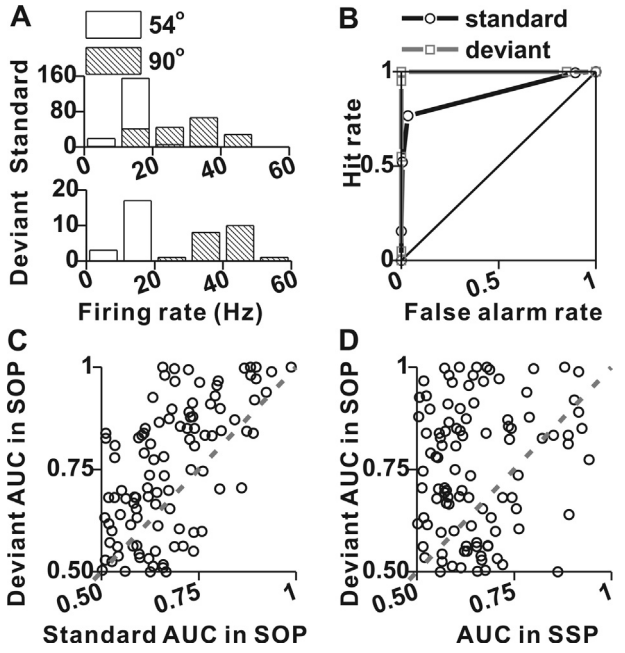

Fig. 5. Spatial SSA enhances the spatial discriminability for deviant locations. (A) Firing rate distribution for responses at standard (top panel) and deviant (bottom panel) locations from the example neuron in Fig. 1. (B) The corresponding ROC curves for deviant locations (gray square) and standard locations (black circle). (C) Scatter plot showing the relationship between AUC of deviant locations and the AUC of the same locations when presented as the standard locations (n = 102) in the location combination [54°, 90°]. The dashed line is the unity slope. (D) Scatter plot showing the relationship between AUC of deviant locations from SOP and the AUC of the same locations in SSP. n = 102.

indicating that the effect of one stimulus on the other responses was the similar to the effect of the versus (Fig. 3A); but when Δf /ΔI became small, the symmetry along the unitary line disappeared. Those neurons had negative SI_1 and positive SI_2, paralleling findings in the frequency domain when the difference in the two frequencies is relatively small (Ulanovsky et al., 2003; Malmierca et al., 2009; Antunes et al., 2010). In the spatial SSA, the SI at the contralateral location was much greater than the SI at the ipsilateral location (Fig. 3B, C). The similarity between the spatial SSA and the frequency SSA suggested that they may share similar neuronal mechanisms.

Specific and non-specific adaptation

SSA is defined as reduced responding to a common stimulus that does not generalize to other rare stimuli (Movshon and Lennie, 1979). It is generally accepted that the response is regarded as SSA only when both deviant responses are stronger compared to their respective standard response. Under this criterion, neurons with both positive SIs have been regarded as exhibiting SSA: Thus, strong spatial SSA occurs for [−90°, 90°] (Fig. 3A), while only 35.1% (20/57; Fig. 3B) and 37.3% (38/102; Fig. 3C) of the neurons show spatial SSA for [18°, 90°] and [54°, 90°], respectively.

On the other hand, non-specific adaptation such as firing-rate adaptation (Westerman and Smith, 1984) or neuronal fatigue (Carandini, 2000), depends on the neurons' history of activity. We observed hints that such non-specific adaptation influences the results in Fig. 3B, C. It seems that there is an asymmetry in the SIs, with higher SIs for a contralateral stimulus (90°). This is generally expected from non-specific adaptation: the contralateral stimulus gives rise to more spikes and therefore, the contralateral response is expected to be less adapted (i.e. larger SI) when embedded in a sequence of less powerful stimuli such as 18° and 54°. This has also been shown in the intensity oddball (Duque et al., 2016). As a result of this non-specific adaptation, the response of the deviant is sensitive to the strength of the response to the standard. Although control paradigms have been introduced to partially separate these two kinds of adaptation (Taaseh et al., 2011), it is still impossible to completely segment the two components in the responses. When specific adaptation occurs, it does not preclude an additional non-specific adaptation component, and similarly, when neurons exhibit non-specific adaptation—as in the data points lying beyond the first quadrant in the scatter plot (Fig. 3A–C) — a specific adaptation component cannot be ruled out.

In the [54°, 90°] combination, for instance, although SSA seems small, there was still strong correlation between the degree of adaptation (CSI) and the spatial discrimination (AUC) of the deviant location (Fig. 8), suggesting that spatial SSA does shape the spatial discrimination. Nonetheless, we do not deny the possibility that non-specific adaptation also played a role. Yet despite the large difference in the strength of spatial SSA between the three location combinations (Fig. 3A–C), our main finding that adaptation increased spatial discriminability and escalated RD for deviant locations holds true for all three situations. As a result, we cannot delineate the difference between the specific and non-specific adaptation.

Context dependent activity in TRN

Spatial context dependent activity has not yet to be studied in great detail. So far, it has mainly been described with close-field spatial cues in inferior colliculus (IC; Dahmen et al., 2010). It has never been addressed in TRN. TRN is comprised of GABAergic (gamma-aminobutyric acid) neurons, receives inputs from corticothalamic and thalamocortical axon collaterals, and projects back to thalamus (Jones, 1975; Houser et al., 1980; Yen et al., 1985). TRN neurons are capable of interacting via electrical synapses (Landisman et al., 2002) or predominantly via GABAergic chemical synapses (Ohara, 1988; Ulrich and Huguenard, 1996).

TRN can enhance or suppress thalamic neuronal activity through its SSA in the frequency domain (Yu et al., 2009b). TRN's enhancing and suppressive effects are believed to be mediated by disinhibitory and inhibitory inputs to the thalamus (Jones, 1975; Houser et al., 1980; Yen et al., 1985; Ohara, 1988; Ulrich and Huguenard, 1996), respectively. Spatial SSA and spatial context dependent firing in TRN may also provide disinhibitory

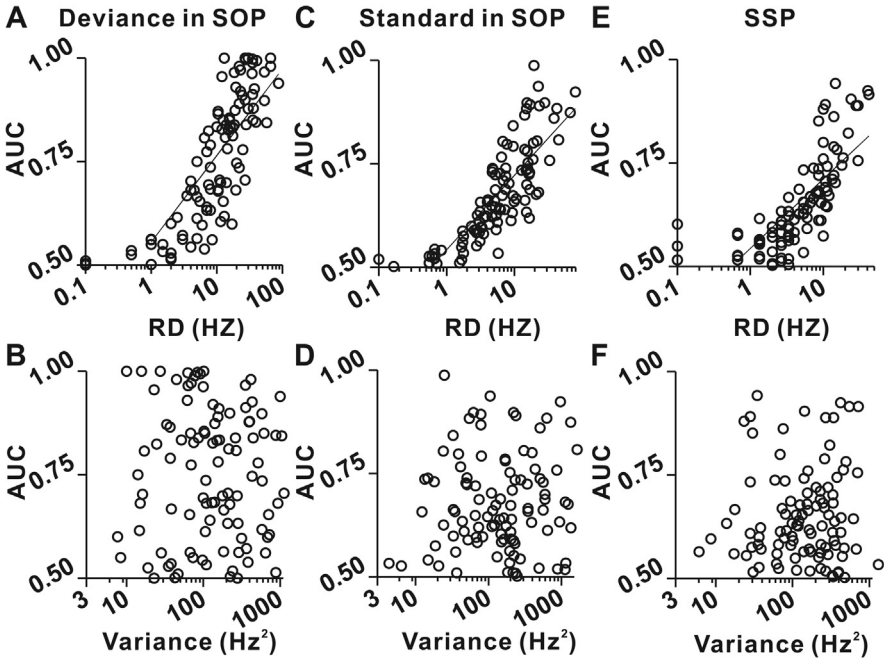

Fig. 6. Parameters influencing spatial discriminability. Dependence of AUC on RD between two locations (top row) and their mean variance (bottom row) for deviant locations (A, B) and standard locations (C, D) in SOP, and in SSP (E, F). Variance is a mean value of two variances computed from two firing distributions at two locations, like those in Fig. 5A. RD was forced to 0.1 if it was smaller than 0.1 for the convenience of illustration on a logarithmic scale. Solid lines illustrate type II linear regression through all data. All the data in SOP are from the location combination [54°, 90°].

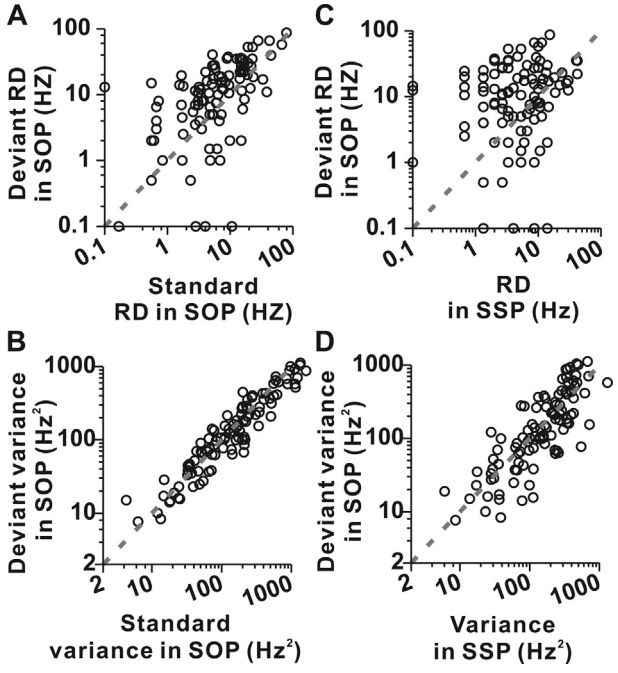

Fig. 7. Factors increasing deviant spatial discriminability. (A, B) Scatter plots show the relationship between deviant RD and standard RD (A), and their corresponding variance (B). (C, D) Scatter plots show the relationship between deviant RD and RD of the same locations in SSP (C), along with their corresponding variance (D). The dashed line in each plot is the unity slope. All the data in SOP are from the location combination [54°, 90°].

and inhibitory input to thalamus and enhance or suppress the thalamic neuronal activity, and if so, would subsequently affect cortical neuron activity (Halassa et al., 2011).

TRN neurons discharge in two activity modes with respect to animal arousal state (Mukhametov et al., 1970; Steriade et al., 1986; Spreafico et al., 1988; Weyand et al., 2001). When the animals are awake, TRN neurons display ‘‘single spike” activity, referred to as tonic mode firing. During slow wave sleep or under drowsiness conditions, TRN neurons switch instead to burst mode firing, characterized by sporadically grouped discharges and interspersed with periods of relative quiescence (Mukhametov et al., 1970; Steriade et al., 1986). The sensory-evoked response in TRN is also dependent on the foregoing spontaneous firing mode (Hartings et al., 2003). Previous investigations found that TRN action was related to behavioral states (Halassa et al., 2014) and was very sensitive to stimulus history with fast adaptation to repetitive stimuli (Yu et al., 2009a). We also previously demonstrated that TRN neuronal activity was dependent on the frequency context and showed SSA in the frequency domain (Yu et al., 2009b). This finding has been extended here, showing that TRN firing was also dependent on the sound’s spatial context. Given the fact that TRN neurons are highly modulated by brain states, the finding that TRN neurons in awake subjects still exhibit significant SSA is also very interesting (Fig. 2 and Fig. 3A), and demonstrates that spatial SSA is not

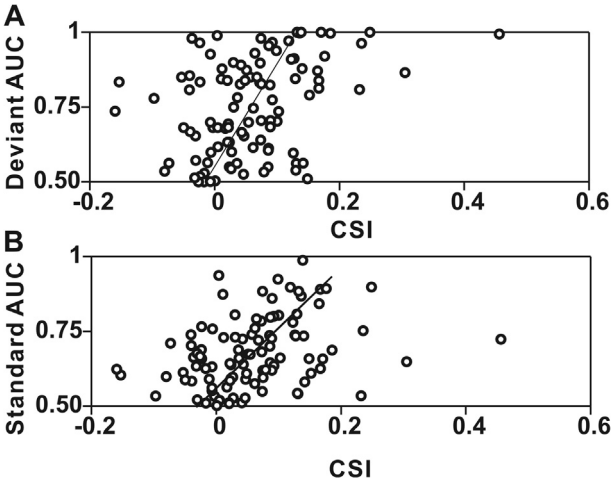

Fig. 8. Relationship between spatial discriminability and the strength of spatial SSA. Scatter plot shows the relationship between CSI and AUC for deviant (A), and standard location (B). All the data are from the location combination [54°, 90°].

simply an artifact of anesthetic use as suggested by Duque and Malmierca (2015).

Spatial discriminability was correlated with the depth of neuronal SSA (Fig. 8), which was very similar to frequency SSA (Von Der Behrens et al., 2009; Ayala et al., 2012) and implies that SSA could dynamically change neuronal discriminability based on both frequency and spatial context. Anatomically, a single TRN neuron receives a large amount of inputs from the thalamus, the cortex and even across modalities (Yu et al., 2011; Gutfreund, 2012), suggesting that a single auditory TRN neuron could sample a lot of context. Context-dependent firing would enable TRN to flexibly gate information from the thalamus to the cortex.

Effect of spatial adaptation on neuronal response variability and response contrast

The role of trial-to-trial variability in neural coding remains an important problem in system neuroscience. A previous report indicated that adaptation could increase neuronal response variability in anesthetized rats (Adibi et al., 2013). The current research suggested that spatial adaptation not only shaped the variability but also modified the response contrast. Within the frequency domain, SSA has been found to improve the neuronal discrimination of deviant stimuli in the auditory cortex (AC; Von Der Behrens et al., 2009) and IC (Ayala et al., 2012). Importantly, however, these studies did not reveal the factors that led to the increased sensitivity for deviant stimuli. This study showed that SSA increased the spatial sensitivity similarly to the frequency domain, and identified RD increase as the primary source for the sensitivity improvement.

RD escalation implies that the slope (or the steepness) of the tuning curve for the deviant location would become sharper, and the slope is always related to the neuronal discrimination threshold (Yu et al., 2012, 2014, 2015). It is therefore likely that spatial adaptation reduces the neuronal discrimination threshold for deviant positions to increase psychological sensitivity.

CONFLICTS OF INTEREST

None.

AUTHOR CONTRIBUTIONS

All authors contributed to the final version of the manuscript. X.X., Y.Z., X.K. and X.Y. designed the experiments, analyzed and interpreted the data; X.X., Y. Z. and X.K. collected and analyzed the data. All authors approved the final version of the manuscript.

FUNDING

This work was supported by National Natural Science Foundation of China (31671081).

Acknowledgements—We are grateful to Dr. Josef Rauschecker, Dr. Anna Wang Roe, and Dr. Lixia Gao for help with revision of the manuscript.

REFERENCES

Adibi M, McDonald JS, Clifford CW, Arabzadeh E (2013) Adaptation improves neural coding efficiency despite increasing correlations in variability. J Neurosci 33:2108–2120.

Aghamolaei M, Zarnowiec K, Grimm S, Escera C (2016) Functional dissociation between regularity encoding and deviance detection along the auditory hierarchy. Eur J Neurosci 43:529–535.

Anderson LA, Malmierca MS (2013) The effect of auditory cortex deactivation on stimulus-specific adaptation in the inferior colliculus of the rat. Eur J Neurosci 37:52–62.

Anderson LA, Christianson GB, Linden JF (2009) Stimulus-specific adaptation occurs in the auditory thalamus. J Neurosci 29:7359–7363.

Antunes FM, Malmierca MS (2014) An overview of stimulus-specific adaptation in the auditory thalamus. Brain Topogr 27:480–499.

Antunes FM, Nelken I, Covey E, Malmierca MS (2010) Stimulus-specific adaptation in the auditory thalamus of the anesthetized rat. PLoS One 5.

Ayala YA, Malmierca MS (2012) Stimulus-specific adaptation and deviance detection in the inferior colliculus. Front Neural Circuits.

Ayala YA, Malmierca MS (2015) Cholinergic modulation of stimulus-specific adaptation in the inferior colliculus. J Neurosci 35:12261–12272.

Ayala YA, Perez-Gonzalez D, Duque D, Nelken I, Malmierca MS (2012) Frequency discrimination and stimulus deviance in the inferior colliculus and cochlear nucleus. Front Neural Circuits 6:119.

Bäuerle P, von der Behrens W, Kössl M, Gaese BH (2011) Stimulus-specific adaptation in the gerbil primary auditory thalamus is the result of a fast frequency-specific habituation and is regulated by the corticofugal system. J Neurosci 31:9708–9722.

Carandini M (2000) Visual cortex: Fatigue and adaptation. Curr Biol 10:R605–R607.

Crick F (1984) Function of the thalamic reticular complex: the searchlight hypothesis. Proc Natl Acad Sci U S A 81:4586–4590.

Dahmen JC, Keating P, Nodal FR, Schulz AL, King AJ (2010) Adaptation to stimulus statistics in the perception and neural representation of auditory space. Neuron 66:937–948.

Duque D, Malmierca MS (2015) Stimulus-specific adaptation in the inferior colliculus of the mouse: anesthesia and spontaneous activity effects. Brain Struct Funct 220:3385–3398.

Duque D, Malmierca MS, Caspary DM (2014) Modulation of stimulus-specific adaptation by GABAA receptor activation or blockade in the medial geniculate body of the anaesthetized rat. J Physiol 592:729–743.

Duque D, Pérez-González D, Ayala YA, Palmer AR, Malmierca MS (2012) Topographic distribution, frequency, and intensity dependence of stimulus-specific adaptation in the inferior colliculus of the rat. J Neurosci 32:17762–17774.

Duque D, Wang X, Nieto-Diego J, Krumbholz K, Malmierca MS (2016) Neurons in the inferior colliculus of the rat show stimulus-specific adaptation for frequency, but not for intensity. Sci Rep 6:24114.

Farley BJ, Quirk MC, Doherty JJ, Christian EP (2010) Stimulus-specific adaptation in auditory cortex is an NMDA-independent process distinct from the sensory novelty encoded by the mismatch negativity. J Neurosci 30:16475–16484.

Gutfreund Y (2012) Stimulus-specific adaptation, habituation and change detection in the gaze control system. Biol Cybern:1–12.

Halassa MM, Siegle JH, Ritt JT, Ting JT, Feng G, Moore CI (2011) Selective optical drive of thalamic reticular nucleus generates thalamic bursts and cortical spindles. Nat Neurosci 14:1118–1120.

Halassa MM, Chen Z, Wimmer RD, Brunetti PM, Zhao S, Zikopoulos B, Wang F, Brown EN, Wilson MA (2014) State-dependent architecture of thalamic reticular subnetworks. Cell 158:808–821.

Hartings JA, Temereanca S, Simons DJ (2003) State-dependent processing of sensory stimuli by thalamic reticular neurons. J Neurosci 23:5264–5271.

Houser CR, Vaughn JE, Barber RP, Roberts E (1980) GABA neurons are the major cell type of the nucleus reticularis thalami. Brain Res 200:341–354.
Jones EG (1975) Some aspects of the organization of the thalamic reticular complex. J Comp Neurol 162:285–308.
Khouri L, Nelken I (2015) Detecting the unexpected. Curr Opin Neurobiol 35:142–147.
Landisman CE, Long MA, Beierlein M, Deans MR, Paul DL, Connors BW (2002) Electrical synapses in the thalamic reticular nucleus. J Neurosci 22:1002–1009.
Malmierca MS, Cristaudo S, Pérez-González D, Covey E (2009) Stimulus-specific adaptation in the inferior colliculus of the anesthetized rat. J Neurosci 29:5483–5493.
Malmierca MS, Sanchez-Vives MV, Escera C, Bendixen A (2014) Neuronal adaptation, novelty detection and regularity encoding in audition. Front Syst Neurosci 8:111.
McAlonan K, Cavanaugh J, Wurtz RH (2008) Guarding the gateway to cortex with attention in visual thalamus. Nature 456:391–394.
Movshon JA, Lennie P (1979) Pattern-selective adaptation in visual cortical neurones. Nature 278:850–852.
Mukhametov LM, Rizzolatti G, Tradardi V (1970) Spontaneous activity of neurones of nucleus reticularis thalami in freely moving cats. J Physiol 210:651–667.
Näätänen R, Gaillard AWK, Mäntysalo S (1978) Early selective-attention effect on evoked potential reinterpreted. Acta Psychol 42:313–329.
Näätänen R, Paavilainen P, Rinne T, Alho K (2007) The mismatch negativity (MMN) in basic research of central auditory processing: A review. Clin Neurophysiol 118:2544–2590.
Nieto-Diego J, Malmierca MS (2016) Topographic distribution of stimulus-specific adaptation across auditory cortical fields in the anesthetized rat. PLoS Biol 14:e1002397.
Ohara PT (1988) Synaptic organization of the thalamic reticular nucleus. J Electron Microscopy Technique 10:283–292.
Pérez-González D, Hernández O, Covey E, Malmierca MS (2012) GABA A-mediated inhibition modulates stimulus-specific adaptation in the inferior colliculus. PLoS One 7.
Paxinos G, Watson C (2005) The rat brain in stereotaxic coordinates. Amsterdam: Elsevier Academic Press.
Reches A, Gutfreund Y (2008) Stimulus-specific adaptations in the gaze control system of the barn owl. J Neurosci 28:1523–1533.
Schwarz C, Hentschke H, Butovas S, Haiss F, Stüttgen MC, Gerdjikov TV, Bergner CG, Waiblinger C (2010) The head-fixed behaving rat–procedures and pitfalls. Somatosens Mot Res 27:131–148.
Spreafico R, de Curtis M, Frassoni C, Avanzini G (1988) Electrophysiological characteristics of morphologically identified reticular thalamic neurons from rat slices. Neuroscience 27:629–638.
Steriade M, Domich L, Oakson G (1986) Reticularis thalami neurons revisited: activity changes during shifts in states of vigilance. J Neurosci 6:68–81.
Szymanski FD, Garcia-Lazaro JA, Schnupp JWH (2009) Current source density profiles of stimulus-specific adaptation in rat auditory cortex. J Neurophysiol 102:1483–1490.
Taaseh N, Yaron A, Nelken I (2011) Stimulus-specific adaptation and deviance detection in the rat auditory cortex. PLoS One 6.
Ulanovsky N, Las L, Nelken I (2003) Processing of low-probability sounds by cortical neurons. Nat Neurosci 6:391–398.
Ulrich D, Huguenard JR (1996) GABAB receptor-mediated responses in GABAergic projection neurones of rat nucleus reticularis thalami in vitro. J Physiol 493(Pt. 3):845–854.
Villa AE (1990) Physiological differentiation within the auditory part of the thalamic reticular nucleus of the cat. Brain Res Brain Res Rev 15:25–40.
Von Der Behrens W, Bäuerle P, Kössl M, Gaese BH (2009) Correlating stimulus-specific adaptation of cortical neurons and local field potentials in the awake rat. J Neurosci 29:13837–13849.
Weese GD, Phillips JM, Brown VJ (1999) Attentional orienting is impaired by unilateral lesions of the thalamic reticular nucleus in the rat. J Neurosci 19:10135–10139.
Westerman LA, Smith RL (1984) Rapid and short-term adaptation in auditory nerve responses. Hear Res 15:249–260.
Weyand TG, Boudreaux M, Guido W (2001) Burst and tonic response modes in thalamic neurons during sleep and wakefulness. J Neurophysiol 85:1107–1118.
Xu X, Yu X, He J, Nelken I (2014) Across-ear stimulus-specific adaptation in the auditory cortex. Front Neural Circuits 8.
Yen CT, Conley M, Hendry SH, Jones EG (1985) The morphology of physiologically identified GABAergic neurons in the somatic sensory part of the thalamic reticular nucleus in the cat. J Neurosci 5:2254–2268.
Yu X-J, Dickman JD, Angelaki DE (2012) Detection thresholds of macaque otolith afferents. J Neurosci 32:8306–8316.
Yu X-J, Meng XK, Xu XX, He J (2011) Individual auditory thalamic reticular neurons have large and cross-modal sources of cortical and thalamic inputs. Neuroscience 193:122–131.
Yu X-J, Xu XX, Chen X, He S, He J (2009a) Slow recovery from excitation of thalamic reticular nucleus neurons. J Neurophysiol 101:980–987.
Yu X-J, Thomassen JS, Dickman JD, Newlands SD, Angelaki DE (2014) Long-term deficits in motion detection thresholds and spike count variability after unilateral vestibular lesion. J Neurophysiol 112:870–889.
Yu XJ, Xu XX, He S, He J (2009b) Change detection by thalamic reticular neurons. Nat Neurosci 12:1165–1170.
Yu XJ, Dickman JD, DeAngelis GC, Angelaki DE (2015) Neuronal thresholds and choice-related activity of otolith afferent fibers during heading perception. Proc Natl Acad Sci U S A 112:6467–6472.
Zhao L, Liu Y, Shen L, Feng L, Hong B (2011) Stimulus-specific adaptation and its dynamics in the inferior colliculus of rat. Neuroscience 181:163–174.

(Received 1 June 2017, Accepted 12 September 2017)
(Available online 20 September 2017)